ELSEVIER

Journal of Alloys and Compounds 461 (2008) 516–520

Journal of ALLOYS AND COMPOUNDS

www.elsevier.com/locate/jallcom

Effect of the morphology on thermal stability of the Ba-Ce-Mn-Al-O oxides synthesized in a reverse microemulsion

Fei Teng [a], Yi Man [a], Shuhui Liang [a], Buergen Gaugue [a], Yongfa Zhu [a,*], Wei Han [b], Zheming Wang [b], Ping Xu [b], Guoxing Xiong [b], Zhijian Tian [b]

[a] *Department of Chemistry, Tsinghua University, Beijing 100084, China*

[b] *State Key Laboratory of Catalysis, Dalian Institute of Chemical Physics, Chinese Academy of Sciences, Dalian 116023, China*

Received 5 March 2007; received in revised form 10 July 2007; accepted 14 July 2007

Available online 19 July 2007

Abstract

Ba-Ce-Mn-Al-O (0.5/0.5/1/11, molar ratios) oxides nanorods and nanoparticles were synthesized in reverse microemulsions. The thermal stabilities and catalytic properties of CH_4 combustion over Ce-Ba-Mn-Al-O samples with different morphologies were investigated. The results showed that the particle morphology had a significant effect on the properties of the catalysts. The rodlike catalyst had higher thermal stability and catalytic activity for methane combustion than the spherical one. A geometric stacking model was proposed to explain the effect.

Keywords: Reverse microemulsion; Morphology; Thermal stability; Methane combustion

1. Introduction

High-temperature catalytic combustion of CH_4 has many advantages over conventional thermal combustion in reducing emissions (NO_x, CO) and enhancing energy efficiency [1–7]. In 2000, Ying and Zarur [8] have prepared $BaAl_{12}O_{19}$ and $CeO_2/BaAl_{12}O_{19}$ catalysts, which have high surface areas and activities. They also prepared the belt-like $BaAl_{12}O_{19}$, but the activity of the belt-like catalyst was not reported. However, designing and synthesizing of the catalysts with high activity and stability is still a challenge to researchers in the field. Recently, Li et al. have reported that single crystalline CeO_2 nanorods had a higher activity for CO oxidation than the nanoparticles. They attributed to the well-defined reactive crystal plane for single crystalline CeO_2 nanorods [9]; whereas they did not report the effect of particle shape on the catalyst properties. It is important for us to research the relationship between the morphology and properties of catalysts.

In this work, the generic Ba-Ce-Mn-Al-O mixed oxide catalysts with different morphologies were synthesized in the reverse microemulsions, using the inexpensive inorganic salts as precursors. The samples were characterized by TEM, XRD, TG–DTA and N_2 adsorption isotherm. The effect of morphology on thermal stability and activity for CH_4 combustion of Ce-Ba-Mn-Al-O catalyst was researched. A geometric stacking model was proposed to explain the effect.

2. Experimental

2.1. Preparation of samples

In the experiment, all the chemicals are of chemical grade and purchased from Beijing Chemicals Company, and were used without further purification. The reverse microemulsion systems used in the study consisted of polyoxyethylene (6) octanyl phenyl alcohol ether ($C_{13}H_{25}O[C_2H_4O]_6H$, MW = 624), *n*-hexanol, cyclohexane and aqueous solution (0.5 M mixture solution of nitrates or 1.0 M $(NH_4)_2CO_3$ solution), which were employed as the surfactant, cosurfactant, continuous phase and dispersed phase, respectively. The weight ratio of aqueous solution in the microemulsion was designated as water content (W_0, wt.%).

Ce-Ba-Mn-Al-O catalyst (Ba/Ce/Mn/Al = 0.5/0.5/1/11, mole ratios) was synthesized by rapidly mixing the same volume of nitrates-containing and $(NH_4)_2CO_3$-containing microemulsion under vigorous stirring at room temperature. The recovered precursor was dried in supercritical ethanol (8.0 MPa, 260 °C). The details of the drying method were illustrated elsewhere [10]. Under flowing air (saturated with water vapor), the dried samples were calcined at

* Corresponding author.
E-mail address: zhuyf@mail.tsinghua.edu.cn (Y. Zhu).

0925-8388/$ – see front matter © 2007 Elsevier B.V. All rights reserved.
doi:10.1016/j.jallcom.2007.07.033

1200 °C for 5 and 10 h, respectively. Typically, the reverse microemulsion at $W_0 = 10$ and 25 was used in the work, respectively. Here, the spherical and rodlike precursors after drying were designated as S0 and R0, respectively; and the calcined Ce-Ba-Mn-Al-O catalysts at 1200 °C for 5 and 10 h were designated as S5, S10 and R5, R10, correspondingly.

2.2. Characterization

The samples were characterized by X-ray diffraction (XRD) on a Rigaku D/MAX-RB X-ray powder diffractometer, using graphite monochromatized Cu Kα radiation ($\lambda = 0.154$ nm), operating at 40 kV and 50 mA. The patterns were scanned from 5° to 70° (2θ) at a scanning rate of 5° min^{-1}. A nitrogen adsorption isotherm was performed at 77 K and $<10^{-4}$ bar on a Micromeritics ASAP2010 gas adsorption analyzer. Each sample was degassed at 200 °C for 5 h before the measurement. Surface area and pore size distribution were calculated by BET (Brunauer–Emmett–Teller) and BJH (Barrett–Joyner–Halenda) methods, respectively. The morphology of the catalyst was characterized with a JEOL model 200CX transmission electron microscope with the accelerating voltage of 200 kV. The powders were dispersed in ethanol ultrasonically, and then the samples were deposited on a thin amorphous carbon film supported by copper grids. TGA–DTA was carried out with Pyris 1 TGA thermogravimeter and DTA-7 (U.S. Perkin-Elmer Co.), and the temperature rises from room temperature to 1300 °C at a rate of 10 °C min^{-1}.

2.3. Catalytic combustion of CH_4

The reaction of methane combustion was carried out in a conventional flow system under atmospheric pressure. The catalysts (1 ml) (20–40 mesh) were loaded in a quartz reactor (i.d. = 10 mm), packed with quartz beads on both top and bottom of the catalyst bed. A mixture gas of methane (1 vol.%) and air (99 vol.%) was fed into the catalyst bed at a gas hourly space velocity (GHSV) of 48,000 h^{-1}. The inlet and outlet gas compositions were analyzed by on-line gas chromatography, using a packed column of carbon molecular sieves and a thermal conductivity detector (TCD). Here, the temperatures at 10 and 90% conversions of methane were designated as T_{10} and T_{90}, respectively, which were used to compare activities of the catalysts.

3. Results and discussion

3.1. Morphologies of Ba-Ce-Mn-Al-O samples

Fig. 1 presents the TEM images of Ba-Ce-Mn-Al-O samples. It is clear that the particle morphologies varied with W_0 values. At $W_0 = 10$, the precursor particles are spherical, and their sizes are about 10 nm (Fig. 1a); at $W_0 = 25$, a network of the fibriform precursor particles was obtained. The particles have 5–10 nm in diameter and 200 nm in length, with aspect ratios of 20–40 (Fig. 1b). The morphology of the precursor particles was most dependent on the original shape of micelle. On the basis of our previous work [10], the shape of micelle varied significantly with W_0. At low W_0 values, the interaction among the micelles was weak, and the micelles were highly dispersed in continuous phase; and the micelles generally maintained spherical morphology. At high W_0 values, the interaction among the micelles became stronger, and the micelles could not maintain regular spherical morphology. As a result, the elongated micelles were formed. Even at higher W_0 values, the micelles interconnected one another to form the bicontinuous structure [11], as shown in Fig. 2. The particles nucleated, grew and organized in the micelles. The micelles controlled the morphology of the particle [12]. Mann and Hopwood [13] have synthesized filament-like barium sulfate particles in microemulsion. After

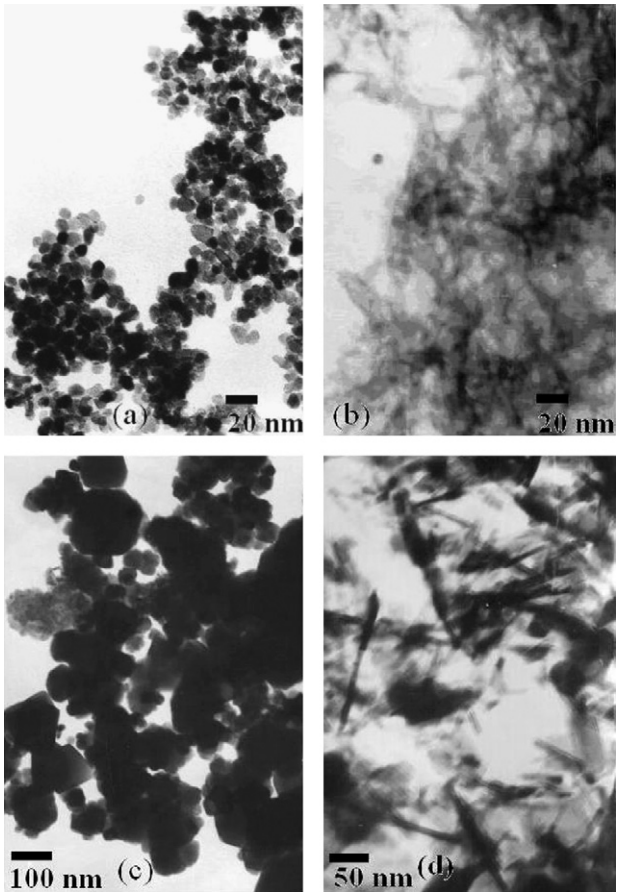

Fig. 1. TEM images of the samples prepared in reverse microemulsions at different water contents (W_0): (a) S0, $W_0 = 10$; (b) R0, $W_0 = 25$; (c) S5; (d) R5. S0, S5: spherical precursor before calcination and the catalyst calcined at 1200 °C for 5 h, respectively; R0, R5: rodlike precursor before calcination and the catalyst calcined at 1200 °C for 5 h, respectively. W_0: water content (wt.%) in the reverse microemulsion system.

supercritical drying, the particle morphology was maintained due to the elimination of the capillary force of water. In contrast with our previous work [10], these results demonstrated that the catalyst morphology was controlled by the microemulsion microstructure, not relative to the kind of the materials.

After the spherical precursor were calcined at 1200 °C for 5 h, Ba-Ce-Mn-Al-O catalyst sintered or agglomerated severely, and their particle sizes are in the range of 50–200 nm (Fig. 1c);

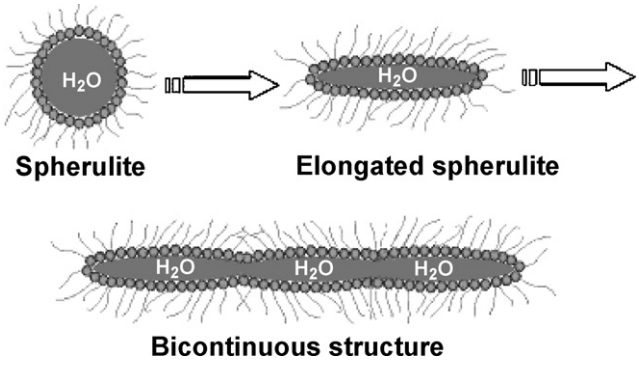

Fig. 2. Variations of the micelle morphology with the increase of W_0.

Table 1
Preparation and properties of Ba-Ce-Mn-Al-O samples

Sample	W_0[a] (wt.%)	Morphology	S_{BET}[a] ($m^2\,g^{-1}$)	V_p[a] ($ml\,g^{-1}$)	d_p[a] (nm)
S0	10	Spherical	381.4	0.4416	4.237
S5	–	Spherical	28.8	0.09065	7.702
S10[b]	–	–	8.9	0.05127	1.030
R0	25	Rodlike	310.3	1.2560	16.192
R5	–	Rodlike	47.1	0.5127	17.743
R10[b]	–	–	29.0	0.1483	7.0301

[a] S_{BET}: surface area calculated by BET method; V_p: average pore volume, d_p: average pore size, which were calculated by BJH method.
[b] S10, R10: spherical and rodlike catalysts calcined at 1200 °C for 10 h, respectively.

the rodlike catalyst were obtained from the fibriform precursor, and they have about 10–20 nm in diameter and 200–400 nm in length (Fig. 1d). By comparison, it is clear that the morphology of the catalyst is very similar to that of the corresponding precursor. Such phenomenon has also been observed by Yan et al. [14] while they prepared MgO nanorods from rodlike $Mg(OH)_2$ precursor.

3.2. Textures and phase compositions of Ba-Ce-Mn-Al-O samples

Table 1 gives the textural properties of Ba-Ce-Mn-Al-O samples. Although the surface area (381.4 $m^2\,g^{-1}$) of S0 sample is higher than that of R0 sample (310.3 $m^2\,g^{-1}$), after calcination at 1200 °C for 5 and 10 h, the surface areas of R5 and R10 are 47.1 and 29.0 $m^2\,g^{-1}$, and the surface areas of the S5 and S10 are 28.8 and 8.9 $m^2\,g^{-1}$, respectively. This may indicate that the rodlike particles had a higher capability resistant to sintering than the spherical ones.

Fig. 3 presents XRD patterns of Ce-Ba-Mn-Al-O samples. Before calcination, both of precursor samples are amorphous. No diffraction peaks of carbonates or hydroxides (Al, Mn, Ce and Ba) appear, indicating that all constitutes were homogeneously mixed in the samples. Because the whole reaction is predominated by the matter exchange process between the micelles, the Al, Mn, Ce and Ba species would react with carbonate homogeneously, although the Mn, Ba, Al species have different precipitating rates. Therefore, through processing with the reverse microemulsion, the precursors can achieve the homogeneity at a molecular level. In supercritical drying process, since the interface between liquid and vapor disappeared, the migration of the active species from inner to surface of the pores could be refrained effectively. As a result, the homogeneity of the precursor could be maintained. After calcination at 1200 °C, some interesting features are observed. First, both of catalysts mainly consisted of CeO_2 and γ-Al_2O_3, and no diffraction peaks of Ba and Mn oxides can be found, indicating that these species distributed homogeneously in the samples. Secondly, it could be also observed that only small amounts of hexaaluminate crystals formed. This can be also ascribed as to the compositions and the separating effect of CeO_2, as to be supported by our previous study [15]. It revealed that at $x = 0.5$, the hexaaluminate crystal cannot form during the syntheses of $Ce_xBa_{1-x}MnAl_{11}O_{19}$

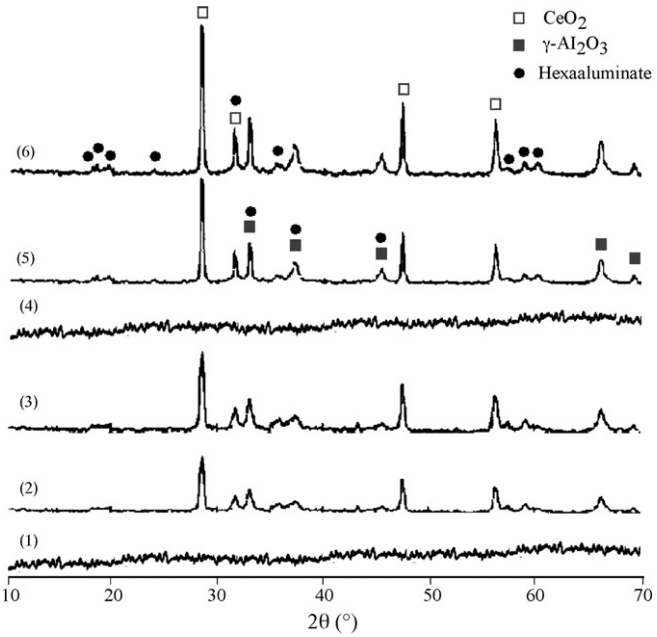

Fig. 3. XRD patterns of Ce-Ba-Mn-Al-O samples: (1) S0, $W_0 = 10$; (2) S5; (3) S10; (4) R0, $W_0 = 25$; (5) R5; (6) R10.

catalysts. Iyi et al. [16] reported that only the mono-, di- and trivalent ions with radius above 1.10 Å could be accommodated in the mirror plane of hexaaluminate crystal. Since the radius of the Ce(III) ion is 1.18 Å, it seems that it could be accommodated in the hexaaluminate lattice. However, after being calcined at 1200 °C in flowing air, the Ce(III) ions would be oxidized into the Ce(IV) ions. The radius of the Ce(IV) ion is 0.92 Å, so Ce would be excluded from the hexaaluminate lattice. Thirdly, the diffraction peaks of α-Al_2O_3 did not appear, indicating that the phase transformation from γ- to α-Al_2O_3 was refrained to some extent. This also is supported by TG–DTA results of both Ce-Ba-Mn-Al-O samples.

Fig. 4 gives TG–DTA curves of Ce-Ba-Mn-Al-O samples prepared at $W_0 = 25$. TG curve of the sample presents two stages of weight loss in the range of 50–600 °C. Below 200 °C, the weight loss of the sample is about 2%, which is caused by the dehydration of the sample; and an endothermal peak at about 100 °C

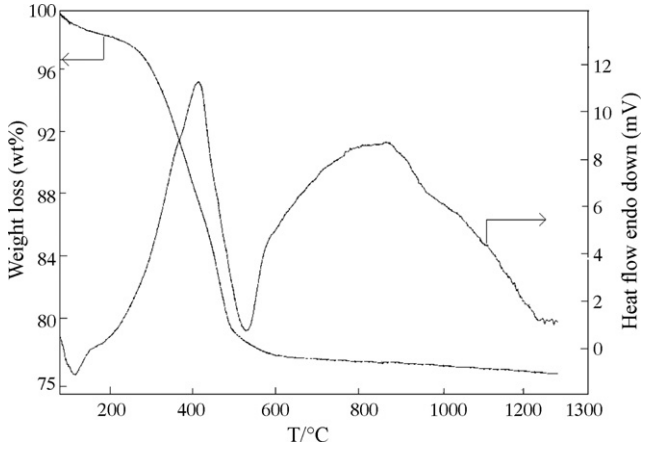

Fig. 4. TG–DTA curves of the Ce-Ba-Mn-Al-O precursor prepared at $W_0 = 25$.

appears in the DTA curve. Between 200 and 600 °C, the weight loss of the sample is about 20%. This may be mainly caused by the removal of organic chemicals and hydroxyls. During the stage, the combustion of the organic chemicals is exothermal since the organic chemicals combusted quickly and generated quantities of heat; but the hydroxylation is endothermal. Ultimately, an exothermal peak could be observed between 200 and 600 °C in the DTA curve. Above 600 °C, almost no weight loss and exothermal peak can be observed in the TG curve and DTA curves, respectively. It is well known that an obvious exothermal peak in DTA curve could generally be observed at 1200 °C due to the phase transformation from γ- to α-Al_2O_3. For this sample, however, no exothermal peak appeared in DTA curve at 1200 °C, indicating phase transformation from γ- to α-Al_2O_3 did not occur.

In our sample, it seems that at high temperatures, the Al diffusion has been refrained by the doping of Ba or Ce. It is generally accepted that γ-Al_2O_3 can be stabilized by the doption of alkaline earth and/or rare earth ions effectively and the stabilizing effect of Ba is more significant among them [17,18]. This may be due to the low mobility of Ba ion, which was closely related to its large radii. The size (1.35 Å) of Ba ion is larger than that (0.92 Å) of Ce(IV) ion. As a result, the phase transformation from γ- to α-Al_2O_3 was delayed significantly. Lastly, the diffraction peaks of CeO_2 and γ-Al_2O_3 crystals in the rodlike catalyst are weaker than those of spherical one, denoting that the rodlike catalyst is composed of smaller crystallites, which is also supported by Scherrer equations.

3.3. Thermal stability of Ba-Ce-Mn-Al-O nanorods

Effect of calcination time on the catalysts with different morphologies was investigated further. When the calcination time was elongated to 10 h, the surface area of spherical catalyst decreased about 69.1%; however, the surface area of the rodlike catalyst decreased about 38.5%. It seems that the spherical catalyst sintered more severely than the rodlike one during the calcination process. In consideration of their similar phase compositions, the difference in capability resistant to sintering of these two catalysts could be related to their different morphologies. Horiuchi et al. [19] have reported that the nucleation of α-Al_2O_3 phase first occurred at the contacting neck between the particles. Because the contacting points between the particles are considered as the nucleating and/or sintering sites, the decrease of contacting chance would suppress the phase transformation and the particle sintering. This indicates that the morphology of the particle had a significant influence on the properties of the materials. Barry and co-workers [20] have also prepared fibrous Al_2O_3 with a high surface area at high temperature and they ascribed the high ability resistant to sintering to the crude structure and fiberform morphology for Al_2O_3 particles. According to the research of Ishikawa et al. [21], the sintering of Al_2O_3 proceeds simultaneously with phase transition from a metastable phase to α-Al_2O_3 at the contacting neck between the particles.

It is well known that the particles with different morphologies have the different stacking tendency. The spherical particles

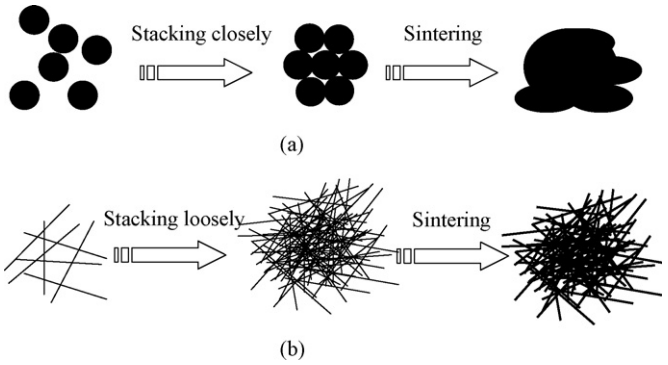

Fig. 5. Schematic diagram of stacking ways for particles with different morphologies: (a) spherical particles and (b) rodlike particles.

have the tendency to stack closely, which means that there are more contacting points among the particles, as shown in Fig. 5a. Therefore, the spherical Ba-Ce-Mn-Al-O particles would sinter severely under the high-temperature calcination. However, it is much difficult to stack closely for the rodlike particles. As shown in Fig. 5b, the rodlike particles have a tendency to form a loose structure, just like cotton, in which the contacting chances of the particles could be reduced greatly. Indeed, it could be supported by the fact that the rodlike sample had the larger pore size and pore volume (16.192 nm, 1.2560 ml g^{-1}) than those (4.237 nm and 0.4416 ml g^{-1}) of the spherical one. The sintering of the particles was refrained significantly during the calcinations process. As a result, the rodlike Ba-Ce-Mn-Al-O catalyst has a higher surface area than the spherical one after calcination at high temperatures (Table 1). Therefore, it could be assumed that the loose texture of nanorods improved thermal stability of the catalyst effectively.

3.4. Methane combustion over Ce-Ba-Mn-Al-O catalysts

The activities of methane combustion over Ce-Ba-Mn-Al-O catalysts were shown in Fig. 6 and summarized in Table 2. After calcination for 5 h, the ignition temperature (T_{10}) and the com-

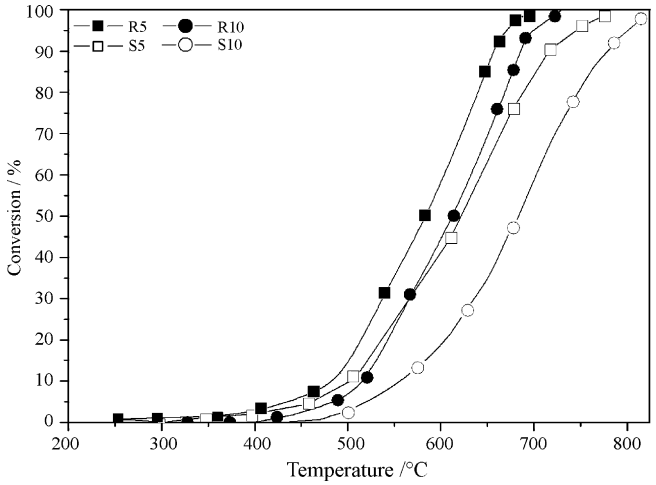

Fig. 6. Light-off curves of methane combustion over Ce-Ba-Mn-Al-O catalysts. *Reaction condition*: GHSV (gas hourly space velocity) = 48,000 h^{-1}, 1 vol.% CH_4, 99 vol.% air.

Table 2
The activities of methane combustion over Ce-Ba-Mn-Al-O catalysts

Catalyst	T_{10} (°C)	ΔT_{10} (°C)	T_{90} (°C)	ΔT_{90} (°C)
S5	500		710	
S10	550	50	770	60
R5	470		650	
R10	520	50	680	30

T_{10}, T_{90}: the temperatures at 10 and 90% conversions of methane, respectively; ΔT_{10}, ΔT_{90}: variations of T_{10} and T_{90}, respectively.

plete combustion temperature (T_{90}) of the rodlike catalyst are ca. 470 and 650 °C, which are 40 and 60 °C lower than those (T_{10} = 500 °C, T_{90} = 710 °C) of the spherical one, respectively. Upon calcination for 10 h, T_{10} and T_{90} of the rodlike catalyst are 520 and 680 °C, respectively, which are lower than those (T_{10} = 550, T_{90} = 770 °C) of the spherical one, respectively. The higher activity of methane combustion over the rodlike catalyst could be ascribed to its higher surface area, larger pore volume and pore size than those of the spherical one (Table 1). Machida et al. [22] have concluded that the high catalytic activity for methane combustion over the $BaMnAl_{11}O_{19}$ catalyst resulted from the fast redox couple between Mn^{2+} and Mn^{3+}. The rodlike catalyst with lager surfaces may provide more active sites than the spherical ones. As a result, the rodlike catalyst shows a higher activity than the latter. It is well known that at low conversions of methane, methane combustion is controlled mainly by surface catalytic reaction; at high conversions of methane, the oxidation of methane usually includes surface reaction and free radical reaction [23]. The free radical reactions are more dependent on mass transfer than on the surface reaction. Before the gases reacted on the solid surface, the gas diffusion from bulk gases to the solid surface occurred. Because the surface reaction is relatively fast, the influence of mass transfer from gas bulk to the catalyst surface on the reaction should not be ignored. The balance between surface reaction and mass transfer may be affected by various factors, e.g., intrinsic activity, particle sizes, porosity and concentration of catalyst, etc. The large surface area of the catalyst is beneficial to mass transfer, since the large surface area may favor for the adsorption of more gases on the solid surface [23]. Therefore, at low methane conversions, the activity of spherical catalyst decreased at the same extent as the rodlike one (ΔT_{10} = 50 °C) upon elongating calcination time; however, at high methane conversion, the activity of spherical catalyst decreased at an extent larger than that of rodlike one (ΔT_{90}: 60 °C versus 30 °C).

4. Conclusions

The properties of the catalysts could be improved effectively by controlling their morphologies. The rodlike catalyst had a higher thermal stability and catalytic activity for methane combustion than the spherical one. It can be expected that the catalysts with excellent performances may be “designed” because of the recent development of morphology-controlled synthesis of nanostructured materials.

Acknowledgements

The financial support from Chinese National Science Foundation (Grant 20433010, 20571047), Chinese Postdoctoral Science Foundation (Grant 20060390057) and the Ministry of Science and Technology of the People’s Republic of China (Grant 1999022401) is gratefully acknowledged.

References

[1] L.D. Pfefferle, W.C. Pfefferle, Catal. Rev. Sci. Eng. 29 (1987) 219.
[2] M. Machida, K. Eguchi, H. Arai, J. Catal. 123 (1990) 477.
[3] G. Groppi, M. Bellotto, C. Cristiani, P. Forzatti, P.L. Villa, Appl. Catal. A 104 (1993) 101.
[4] L. Qi, J. Ma, H. Cheng, Z. Zhao, Colloids Surf. A 108 (1996) 117.
[5] D. Walsh, J.D. Hopwood, S. Mann, Science 164 (1994) 1576.
[6] J. Tanori, M.P. Pileni, Adv. Mater. 7 (1995) 862.
[7] K. Kandori, K. Kon-no, A. Kitahara, J. Colloid Interf. Sci. 11 (1987) 5579.
[8] A.J. Zarur, J.Y. Ying, Nature 403 (2000) 65.
[9] K. Zhou, X. Wang, X. Sun, Q. Peng, Y. Li, J. Catal. 229 (2005) 206.
[10] F. Teng, Z. Tian, J. Xu, G. Xiong, L. Lin, Stud. Surf. Sci. Catal. 147 (2004) 493.
[11] A.J. Zarur, N.Z. Mehenti, A.T. Heibel, J.Y. Ying, Langmuir 16 (2000) 9168.
[12] H. Hoffmann, G. Platz, W. Ulbricht, J. Phys. Chem. 85 (1981) 3160.
[13] J.D. Hopwood, S. Mann, Chem. Mater. 9 (1997) 1819.
[14] L. Yan, J. Zhuang, X. Sun, Z. Deng, Y. Li, Mater. Chem. Phys. 76 (2002) 119.
[15] F. Teng, P. Xu, Z. Tian, G. Xiong, Y. Xu, Z. Xu, L. Lin, Green Chem. 7 (2005) 493.
[16] N. Iyi, S. Takekawa, S. Kimura, J. Solid State Chem. 83 (1989) 8.
[17] J.S. Church, N.W. Cant, D.L. Trimm, Appl. Catal. A 101 (1993) 105.
[18] A. Sepulveda-Escribano, M. Primet, H. Praliand, Appl. Catal. A 108 (1994) 221.
[19] T. Horiuchi, T. Osaki, T. Sugiyama, T. Mori, J. Non-Cryst. Solids 291 (2001) 187.
[20] H. Zhu, J.D. Riches, J.C. Barry, Chem. Mater. 14 (2002) 2086.
[21] T. Ishikawa, R. Ohashi, H. Nakabayashi, A. Ueno, A. Furuta, J. Catal. 134 (1992) 87.
[22] M. Machida, K. Eguchi, H. Arai, J. Catal. 120 (1989) 377.
[23] E.M. Johansson, K.M.J. Danielsson, E. Pocoroba, E.D. Haralson, S.G. Järäs, Appl. Catal. A: Gen. 182 (1999) 199.